Feng, H., et al., 2021, Erosion of the Himalaya-Karakoram recorded by Indus Fan deposits since the Oligocene: Geology, v. 49, https://doi.org/10.1130/G48445.1

Erosion of the Himalaya-Karakoram recorded by Indus Fan deposits since the Oligocene

Han Feng[1], Huayu Lu[1*], Barbara Carrapa[2], Hanzhi Zhang[1], Jun Chen[3], Ying Wang[1] and Peter D. Clift[4]

[1]*School of Geography and Ocean Science, Nanjing University; Key Laboratory of Coast and Island Development, Ministry of Education, Nanjing 210023, China.*

[2]*Department of Geosciences, University of Arizona, Tucson, Arizona 85721, USA.*

[3] *School of Earth Sciences and Engineering, Nanjing University; Key Laboratory of Surficial Geochemistry, Ministry of Education, Nanjing 210023, China.*

[4]*Department of Geology and Geophysics, Louisiana State University, Baton Rouge, LA 70803, USA.*

***** *Correspondence to: huayulu@nju.edu.cn*

METHODS

Heavy minerals analysis

For each bulk sample, the 63–250 μm size fraction was extracted using steel sieves. The heavy minerals were separated using sodium polytungstate (density 2.89 g/cm^3) with help of funnels (Andò et al., 2020). Following the washing and drying, the fractions of heavy minerals were mounted on glass slides with Canada balsam. For each sample, at least 300 transparent heavy minerals were point-counted under a petrographic microscope at the Laboratory of Earth Surface Process and Environment, Nanjing University, using the method described in Mange and Maurer (1992). Heavy-mineral concentrations index (HMC) were calculated based on Garzanti and Andò (2007).

Zircon U-Pb dating

More than 200 zircon and apatite grains for each sample were picked from the residual concentrated heavy minerals using a microscope to ensure statistical adequacy (Andersen, 2005). The grains were then mounted in epoxy resin and polished for dating. U-Pb isotopes of zircons were measured using an Agilent 7700x ICP-MS with a New Wave 193 nm laser ablation system at the Laboratory of Earth Surface Process and Environment, Nanjing University. The laser beam diameter was 30 μm with a 10 Hz repetition rate. Zircon 91500 was used as an external standard for isotopic fractionation correction, while NIST 610 (Pearce et al., 1997) was used as the standard for normalizing the unknown U, Th, and Pb contents. Glitter 4.4.2 (van Achterbergh et al., 2001) was used to process the raw ICP-MS data. Common Pb was corrected following Andersen (2002). Zircon particle ages were obtained using the following protocol: 1) Individual zircon discordance values <15%, in agreement with the concordant ages of published data from

potential sources; 2) $^{206}Pb/^{238}U$ ages were used for zircon grains with ages <1000 Ma and $^{207}Pb/^{206}Pb$ ages for older grains. All zircon U-Pb ages and 1σ uncertainties are reported in Table DR11.

Apatite Fission Track dating

Apatite grains were mounted in epoxy on glass slides, polished and etched in 5.5 M nitric acid for 20 s at 21°C (Donelick et al., 2005) before irradiation at Oregon State University. After irradiation, the mica external detectors were etched in 40% hydrofluoric acid for 15 minutes at 21°C (Donelick et al., 2005). Analyses were conducted for optical identification of fission tracks using an Olympus microscope at 1600× magnification with the drawing tube located above a digitizing tablet and a Kinetek computer-controlled stage driven by the FT Stage program (Dumitru, 1993) at the Fission Track Laboratory of University of Arizona. Apatite fission track ages were calculated using the external detector method (Dumitru, 1993) and are reported in Table DR12.

Nd-Sr isotopic composition

About 1 g of the bulk sample was dissolved in 0.5 mol/L acetic acid overnight to remove the carbonate component, followed by removal of organic matter using 5% H_2O_2. About 0.1 g of the sample was used for Nd-Sr isotope analysis. The samples were digested in a mixture of nitric acid and hydrofluoric acid for 36 h in sealed Teflon vials at 115 °C. The digested solution was then loaded into ion exchange columns to separate Sr and Nd elements using Sr-Spec, Ln-Spec and Tru-Spec resin (Aciego et al., 2009). The determination of Sr and Nd isotopes was performed on a Neptune plus Multi-Collector Inductively Coupled Plasma Mass Spectrometer (MC-ICP-MS) at the MOE Key Laboratory of Surficial Geochemistry, Nanjing University.

Instrumental mass bias for Sr and Nd isotopes was corrected by normalizing the $^{86}Sr/^{88}Sr$ ratio to 0.1194 and the $^{146}Nd/^{144}Nd$ ratio to 0.7219. Sr standard SRM987 and Nd standard JMCNd_2O_3 were periodically measured to check the reproducibility and accuracy of isotopic analyses, with a mean $^{87}Sr/^{86}Sr$ ratio of 0.710239 ± 42 (2σ, n = 10) and a mean $^{143}Nd/^{144}Nd$ ratio of 0.512099 ± 15 (2σ, n = 15). A standard material, BCR-2, was used to verify the chemical procedure. Measurements of ten replicates yielded a mean $^{87}Sr/^{86}Sr$ value of 0.705018 ± 20 (2σ, n = 10) and a mean $^{143}Nd/^{144}Nd$ value of 0.512626 ± 15 (2σ, n = 10). Epsilon Nd values (ε_{Nd}) were calculated using chondritic values of $^{143}Nd/^{144}Nd$ = 0.512638 (Jacobsen and Wasserburg, 1980).

Multi-dimensional scaling analysis

Multi-dimensional scaling (MDS) map is used to illustrate similarities of zircon age distributions of samples (Vermeesch, 2013) in Indus Fan deposits. The dissimilarity or distance between two samples are first defined and calculated based on Kolmogorov–Smirnov test (Feller, 2015):

$$\delta_{i,j} = \max_t \left| F_i(t) - F_j(t) \right|$$

Where $F(t)$ is the empirical cumulative distribution function (CDF) of zircon ages.

A matrix of pairwise dissimilarities is shown as:

$$\delta = \begin{bmatrix} \delta_{1,1} & \delta_{1,2} & \cdots & \delta_{1,n} \\ \delta_{2,1} & \delta_{2,2} & \cdots & \delta_{2,n} \\ \vdots & \vdots & \delta_{i,j} & \vdots \\ \delta_{n,1} & \delta_{n,2} & \cdots & \delta_{n,n} \end{bmatrix}$$

Then a monotonically increasing function f ($\delta_{i,j}$) and a two-dimensional configuration of points $\mathbf{p}=\{p_1,p_2,\ldots,p_i,\ldots,p_j,\ldots,p_n\}$ are introduced, with $p_i = (x^i, y^i)$, $p_j = (x^j, y^j)$ and $1 \leq i,j \leq n$. The Euclidean distance between any two points p_i and p_j in this configuration should be approximated

to the f ($\delta_{i,j}$). According to this, configuration **p** can be found analytically by relatively straightforward linear algebra (Cox and Cox, 2008), and plotted on a MDS map (Fig. DR1).

References

Aciego, S.M., Bourdon, B., Lupker, M., and Rickli, J., 2009, A new procedure for separating and measuring radiogenic isotopes (U, Th, Pa, Ra, Sr, Nd, Hf) in ice cores: Chemical Geology, v. 266, no. 3-4, p. 194–204, doi: 10.1016/j.chemgeo.2009.06.003.

Andersen, T., 2002, Correction of common lead in U–Pb analyses that do not report 204Pb: Chemical Geology, v. 192, no. 1-2, p. 59–79, doi: 10.1016/S0009-2541(02)00195-X.

Andersen, T., 2005, Detrital zircons as tracers of sedimentary provenance: limiting conditions from statistics and numerical simulation: Chemical Geology, v. 216, no. 3-4, p. 249–270, doi: 10.1016/j.chemgeo.2004.11.013.

Andò, S., 2020, Gravimetric Separation of Heavy Minerals in Sediments and Rocks: Minerals, v. 10, no. 3, p. 273–15, doi: 10.3390/min10030273.

Cox, M.A.A., and Cox, T.F., 2008, Multidimensional Scaling, in Handbook of Data Visualization, Springer Berlin Heidelberg, Berlin, Heidelberg, p. 315–347.

Donelick, R.A., O'Sullivan, P.B., and Ketcham, R.A., 2005, Apatite Fission-Track Analysis: Reviews in Mineralogy and Geochemistry, v. 58, no. 1, p. 49–94, doi: 10.2138/rmg.2005.58.3.

Dumitru, T.A., 1993, A new computer-automated microscope stage system for fission-track analysis: Nuclear Tracks and Radiation Measurements, v. 21, no. 4, p. 575–580, doi: 10.1016/1359-0189(93)90198-I.

Feller, W., 2015, On the Kolmogorov–Smirnov Limit Theorems for Empirical Distributions, in Selected Papers I, Springer International Publishing, Cham, p. 735–749.

Garzanti, E., and Andò, S., 2007, Heavy Mineral Concentration in Modern Sands: Implications for Provenance Interpretation, in Heavy Minerals in Use, Developments in Sedimentology, Elsevier, p. 517–545.

Jacobsen, S.B., and Wasserburg, G.J., 1980, Sm-Nd isotopic evolution of chondrites: Earth and Planetary Science Letters, v. 50, no. 1, p. 139–155, doi: 10.1016/0012-821X(80)90125-9.

Mange, M.A., and Maurer, H.F.W., 1992, Heavy Minerals in Colour: Springer, Dordrecht.

Pearce, N.J.G., Perkins, W.T., Westgate, J.A., Gorton, M.P., Jackson, S.E., Neal, C.R., and Chenery, S.P., 1997, A Compilation of New and Published Major and Trace Element Data for NIST SRM 610 and NIST SRM 612 Glass Reference Materials: Geostandards Newsletter, v. 21, p. 115–144, doi: 10.1111/j.1751-908X.1997.tb00538.x.

Van Achterbergh, E., Ryan, C.G., Jackson, S.E., and Griffin, W.L., 2001, Data reduction software for LA-ICP-MS, in Sylvester, P.J. ed., Laser-ablation-ICPMS in the earth sciences: Principles and applications (Short course series), Ottawa, p. 239–243.

Vermeesch, P., 2013, Multi-sample comparison of detrital age distributions: Chemical Geology, v. 341, p. 140–146, doi: 10.1016/j.chemgeo.2013.01.010.

AGE CONTROL

The chronology of Sites 722 and 731 was established based on the Initial Reports for ODP Sites 722 and 731 (Shipboard Scientific Party, 1989a, 1989b; Prell and Niitsuma, 1989). The upper parts of Sites 722 and 731 (< ~15 Ma) have adequate fossil assemblages and paleomagnetic data, as indicated in the Initial Report (Fig. 1D and Table DR1) (Prell and Niitsuma, 1989). The lower parts (> ~15 Ma) of Sites 722 and 731 have few fossil assemblage data and no paleomagnetic data, and thus there is no age control proposed in Prell and Niitsuma (1989). We first updated the reported age controls of the upper parts of Sites 722 and 731 according to Gradstein (2012), and then, estimated the age controls in the lower part based on the nannofossil assemblage events that were reported by Shipboard Scientific Party, 1989a, 1989b.

For Site 722, the deepest age control point reported in the Initial Report was 13.8 Ma, which was obtained from the 'T *Globorotalia peripheronda*' faunal event (here, 'T' denotes 'Top limit') at the depth of 391.80–393.86 mbsf (meters below the sea floor). Below this depth, the Initial Report indicate that the sediments at 565.6 mbsf contained the nannofossil species *Sphenolithus belemnos* (17.95-19.03 Ma) and *Discoaster druggi* (17.95-22.82 Ma). Here we use the average of 18.49 Ma for the age range of *Sphenolithus belemnos* (17.95-19.03 Ma) as the age control for a depth of 565.6 mbsf at Site 722. In the same way, the age controls for Site 731 below the lowest reported 'T *Sphenolithus heteromorphus*' faunal event of 13.53 Ma at depths of 299.2-300.35 were obtained according to the Initial Report. Sediments at depths of 371.1 mbsf and 514.4 mbsf both contained *Sphenolithus belemnos* and are thus likely to be within the age range of *Sphenolithus belemnos* (17.95-19.03 Ma). The sediments at the depth of 629.3 mbsf contained *Cyclicargolithus abisectus* (>24.67 Ma) and *Dictyococcites bisectus* (23.13-38.25 Ma), indicating ages older than ~24 Ma. We obtained 24.67 Ma as the age at a depth of 629.3 mbsf.

The nannofossil assemblage at a depth of 807.85 mbsf includes *Cyclicargolithus abisectus* (>24.67 Ma), *Cyclicargolithus floridanus* (>11.85 Ma), *Discoaster deflandrei* (>15.8 Ma), *Helicosphaera euphratis* (14.91-37.32 Ma), *Helicosphaera recta* (22.82-32.92 Ma), and *Sphenolithus ciperoensis* (24.43-29.62 Ma). As 807.85 mbsf is much deeper than 629.3 mbsf and the age of 807.85 mbsf cannot be younger than that of 629.3 mbsf, we took the average rather than the upper limit age of the time range of *Sphenolithus ciperoensis* (24.43-29.62 Ma), which yields the age of 27.03 Ma for the depth of 807.85 mbsf. We then linearly interpolated and extrapolated ages for each sampling depth both between and beyond the estimated age controls (Fig. 1D).

However, the age controls for sediments older than ~24 Ma are extrapolated, because none of the reported nannofossil assemblage in the lower part of the sites has a Last Appearance Datum (LAD) older than 24.43 or 24.67 Ma. Therefore, the age range of strata investigated by this study can be considered as >24-16 Ma.

DECOMPACTION

Decompaction is a technique that restores present-day thicknesses to sedimentary layers during the burial history by use of porosity-depth relationships (Sclater and Christie, 1980; Allen and Allen, 2013). The widely used porosity-depth relation has the form of a negative exponential as:

$$\varphi(y) = \varphi_0 e^{-cy}$$

where φ_0 is the porosity at the surface, y is the depth and c is a coefficient determining the slope of the ϕ-depth curve. The porosity data with depth of ODP site 722 and 731 can be found in the Initial Report for ODP Sites 722 and 731 (Prell and Niitsuma, 1989). We obtained $\varphi_0 =$ 73% and c = 0.001 for the site 722 and $\varphi_0 =$ 64% and c = 0.0008 for Site 731 (Fig. DR2).

Consider a sediment layer at present burial depths of y_1 and y_2 that is to be restored to new shallower depths y_1' and y_2'. The volume of water-filled pore space V_w between depths y_1 and y_2 is simply the porosity integrated over the depth interval:

$$V_w = \int_{y_1}^{y_2} \varphi_0 e^{-cy} \mathrm{d}y$$

which on integration gives:

$$V_w = \frac{\varphi_0}{c}(e^{-cy_1} - e^{-cy_2})$$

The total volume of the sediment layer (V_t) is the volume due to pore-filling water (V_w) and the volume of the sediment grains (V_s):

$$V_s = V_t - V_w$$

Considering a unit cross-sectional area:

$$y_s = y_t - y_w = (y_2 - y_1) - \frac{\varphi_0}{c}(e^{-cy_1} - e^{-cy_2})$$

And the same for the shallower layer y_1' and y_2':

$$y_s{}' = y_t{}' - y_w{}' = (y_2{}' - y_1{}') - \frac{\varphi_0}{c}(e^{-cy_1'} - e^{-cy_2'})$$

Since the volume of the sediment grains remain the same during the decompaction ($y_s = y_s{}'$), thus the restored thickness is:

$$y_2' - y_1' = (y_2 - y_1) - \frac{\varphi_0}{c}(e^{-cy_1} - e^{-cy_2}) + \frac{\varphi_0}{c}(e^{-cy_1'} - e^{-cy_2'})$$

We restored every 1 m of the sedimentary layer of the ODP Site 722 and 731 to the surface and obtained the restored depth for every samples and age controls (Table DR2).

References

Allen, P.A., and Allen, J.R., 2013, Basin Analysis: Principles and Application to Petroleum Play

Assessment: Oxford.

Gradstein, F.M., 2012, Biochronology, in Gradstein, F.M., Ogg, J.G., Schmitz, M.D., and Ogg, G.M. eds., The Geologic Time Scale, Elsevier, Amsterdam, p. 43–61.

Prell, W.L., and Niitsuma, N., 1989, Proceedings of the Ocean Drilling Program, Initial Reports, 117: Ocean Drilling Program, College Station, TX.

Sclater, J.G., and Christie, P.A.F., 1980, Continental stretching: An explanation of the Post-Mid-Cretaceous subsidence of the central North Sea Basin: Journal of Geophysical Research: Solid Earth, v. 85, no. B7, p. 3711–3739, doi: 10.1029/JB085iB07p03711.

Shipboard Scientific Party, 1989a. Site 722. In: Prell, W.L., Niitsuma, N. (Eds.), *Proceedings of the Ocean Drilling Program*, Part A: Initial Reports, 17, Ocean Drilling Program, College Station, TX, pp. 255-317,

Shipboard Scientific Party, 1989b. Site 731. In: Prell, W.L., Niitsuma, N. (Eds.), Proc. ODP, Initial Reports, 117, Ocean Drilling Program, College Station, TX, pp. 585-652, doi:10.2973/odp.proc.ir.117.108.1989.

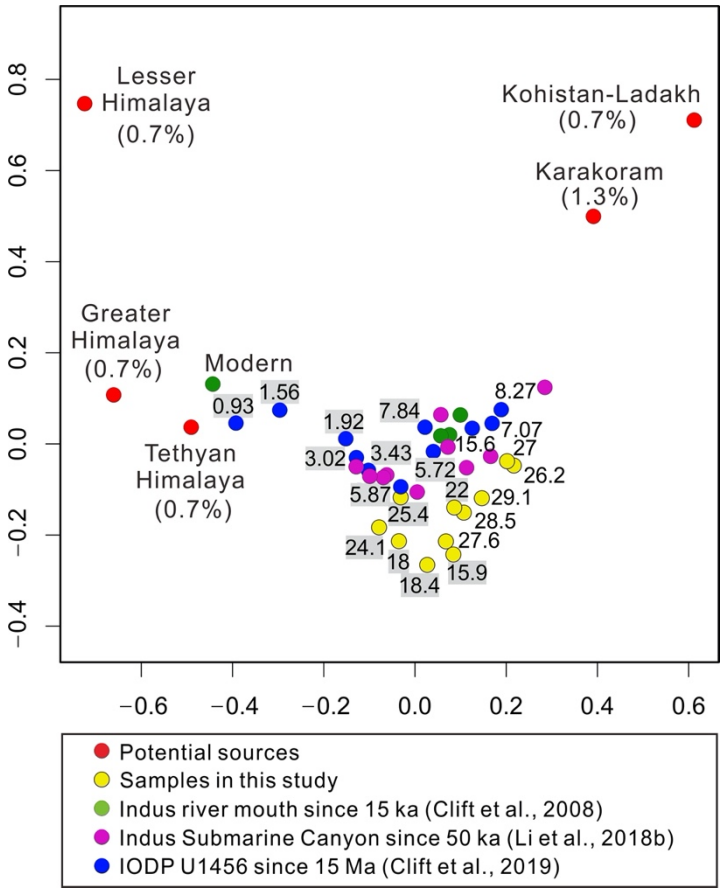

Fig. DR1. Multi-dimensional scalar (MDS) diagram of zircon U-Pb age distributions from Indus Fan deposits dated by this study and previous studies, compared with the potential sources. Concentrations of zircon grains in heavy mineral suits of the sources are labeled as percentage with parentheses (Table DR7); The samples from this study and from IODP Site U1456 were labeled with their depositional ages (Ma). The labels of samples dated at 25-16 Ma and <6 Ma have grey backgrounds, all of which are closer to the Himalayan sources than the others.

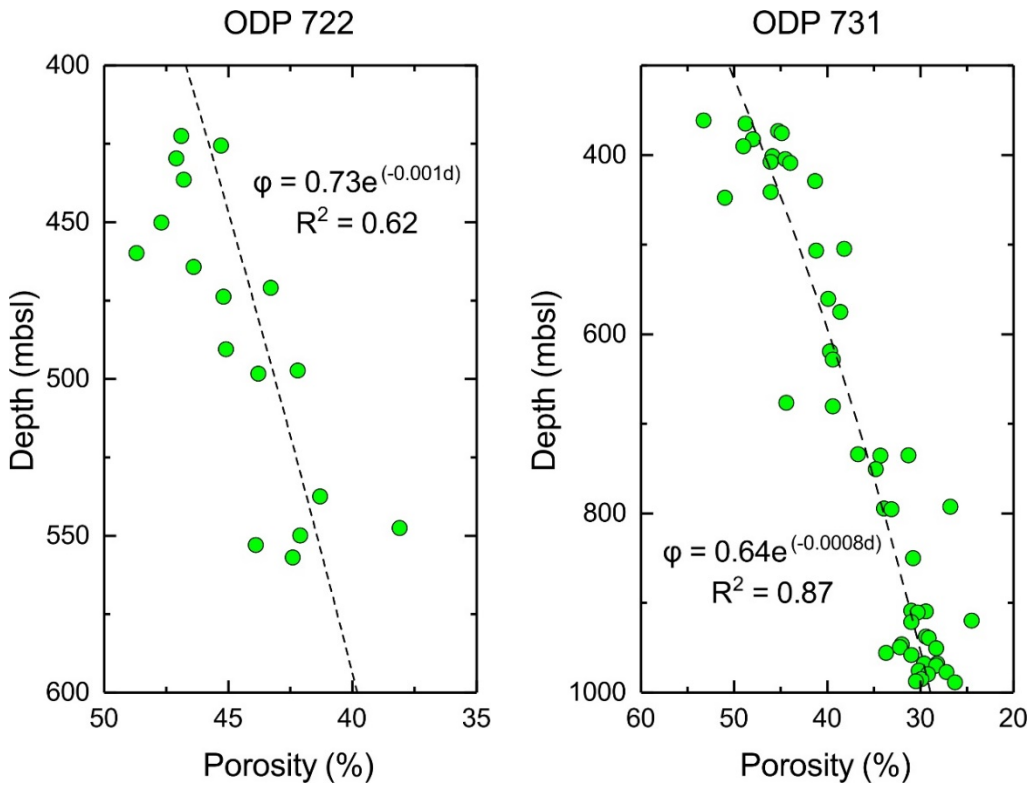

Fig. DR2. Porosity-depth relationship of ODP Sites 722 and 731 for sediments <400 mbsl.

Porosity data are from Prell and Niitsuma (1989).

Table DR1.

Biostratigraphic and magnetostratigraphic age controls for ODP Sites 722 and 731

Depth below the seafloor (mbsl)	Event	Age (Ma)
	ODP Site 722	
5.65	*B* Emiliania huxleyi*	0.29
16.95	*T Pseudoemiliania lacunosa*	0.44
24.75	*B Pterocorys hertwegii*	0.74
31.68	*Tc Reticulofenestra asanoi*	0.91
37.65	*B Jaramillo*	1.07
53.85	*B Gephyrocapsa spp. >4 μm*	1.73
63.14	*T Discoaster brouweri*	1.93
74.35	*T Discoaster pentaradiatus*	2.39
82.45	*Matuyama/Gauss*	2.58
101.55	*T Phormostichoartus fistula*	3.49
115.6	*T Spongaster pentas; B Spongaster tetras tetras*	4.13
134.9	*T Didymocyrtis penultima; B Didymocyrtis avita*	4.24
142.03	*T Sidufjall*	4.80
151	*B Thvera*	5.24
163.9	*T Discoaster quinqueramus*	5.59
178.95	*B Pterocorys campanula; T Siphostichartus corona*	5.67
188.45	*B Pulleniatina primalis*	6.60
208.05	*T Acrobotrys tritubus*	6.34
227.35	*T Calocycletta caepa*	6.14
241.7	*B Solenosphaera omnitubus omnitubus*	7.41
275.6	*T Diartus petterssoni; B Diartus hughesi*	8.84
287.45	*B Neogloboquadrina acostaensis*	9.83
304.7	*T Discoaster hamatus*	9.53
329.35	*T Cyrtocapsella japonica*	9.86

339.05	*B Globoturborotalita nepenthes*	11.63
358.25	*T Fohsella fohsi; Fohsella plexus*	11.79
375.1	*Bc Discoaster kugleri*	11.90
382.41	*T Sphenolithus heteromorphus*	13.53
391.8	*T Fohsella peripheroronda*	13.80
565.6	*Sphenolithus belemnos and Discoaster druggi*	18.49
	ODP Site731	
5.62	*B Emiliania huxleyi*	0.29
18.45	*T Pseudoemiliania lacunosa*	0.44
24.65	*T Anthocyrtidium nosicaae*	0.70
34.15	*B Pterocorys hertwegii*	0.74
45.45	*B Jaramillo*	1.07
56.45	*T Helicosphaera sellii*	1.26
64.45	*T Calcidiscus macintyrei*	1.60
72.35	*T Pterocanium prismatium; Theocorythium ventulum*	2.04
83.85	*T Discoaster brouweri*	1.93
96	*T Discoaster pentaradiatus*	2.39
105.7	*T Spongaster pentas; B Spongaster tetras tetras*	4.13
115.4	*B Stichocorys delmontensis; T Stichocorys peregrina*	7.78
130.35	*B Solenosphaera omnitubus omnitubus*	7.41
140.95	*T Diartus petterssoni; B Diartus hughesi*	8.84
149.75	*T Dictyocoryne ontongensis*	7.94
163.7	*B Discoaster quinqueramus*	8.12
178.75	*T Didymocyrtis laticonus; B Didymocyrtis antepenultima*	8.84
192.8	*B Spongaster berminghami*	8.35
202.5	*T Discoaster hamatus*	9.53
227.25	*T Cyrtocapsella japonica*	9.86
238.75	*B Discoaster hamatus*	10.55
299.2	*T Sphenolithus heteromorphus*	13.53

371.1	*T Sphenolithus belemnos*	17.95
514.4	*B Sphenolithus belemnos*	19.03
629.3	*T Cyclicargolithus abisectus*	24.67
807.85	*Sphenolithus ciperoensis*	27.03

*T = top, Tc = top common, B = bottom, Bc = bottom common

Table DR2.

Sample details including restored depth, interpolated ages and analytical methods

Sample name	Depth (mbsl)	Restored depth (mbsl)	Age (Ma)	Apatite Fission track dating	Zircon U-Pb dating	Heavy mineral analysis	Nd-Sr isotope
722B-50X-1W	470.2	734.4	15.8	√	√	√	√
722B-50X-4W	473.6	742.6	15.9				√
722B-57X-1W	537.2	875.1	17.6				√
722B-58X-1W	547.1	896.7	17.9				√
731A-41X-3W	383.6	479.8	18.0		√	√	
731A-42X-1W	390.8	490.2	18.1				√
731B-3X-1W	428.3	545.8	18.4				√
731B-4X-1W	428.9	547.3	18.4	√	√	√	
731C-2R-1W	503.1	662.7	18.9				√
731C-2R-2W	504.9	665.9	19.0				√
731C-4R-1W	561.2	756.8	21.3				√
731C-5W-4W	575.7	781.7	22.0	√	√	√	√
731C-6R-1W	618.1	852.3	24.1		√		√
731C-7W-3W	631.6	876.3	24.7				√
731C-8R-4W	681.3	961.2	25.3	√	√	√	√
731C-9W-6W	693.1	982.4	25.5				√
731C-11W-1W	745.5	1077.1	26.2		√	√	√
731C-13W-4W	806.8	1188.9	27.0	√	√	√	√
731C-14R-2W	850.7	1271.2	27.6		√	√	√
731C-17R-2W	918.1	1399.3	28.6		√	√	√
731C-22R-1W	965.9	1495.0	29.3	√	√	√	√

Table DR3.

Detrital heavy mineral assemblages of the orogenic belts in sediment provenance in the Indus River drainage basin (Liang et al., 2019)

Tectonic Units	HMC*	Ap and Ttn	Spinel	Px	Am	Grt	HgM	Ep	ZTR	Total
Karakoram	5.7	14	0	8	43	10	1	18	6	100
Ladakh	11.1	8	0	6	78	1	0	5	2	100
Kohistan	37.8	5	0	23	50	1	0	20	1	100
Himalaya	4.8	12	0	13	27	22	10	7	9	100

*HMC = Heavy mineral concentration; Ap = apatite; Ttn = titanite; Px = pyroxene; Am = amphibole; Grt = garnet; HgM = high-grade minerals (staurolite, andalusite, kyanite, sillimanite); Ep = epidote; ZTR = ultrastable minerals (zircon, tourmaline, rutile)

Table DR4.

Nd-Sr isotopic composition of samples from ODP Sites 722 and 731

Sample name	Age (Ma)	$^{143}Nd/^{144}Nd$	SE	ε_{Nd} *	$^{87}Sr/^{86}Sr$	SE
722B-50X-1W	15.8	0.512053	5	-11.42	0.723999	7
722B-50X-4W	15.9	0.512034	11	-11.77	0.727225	8
722B-57X-1W	17.6	0.512075	7	-10.99	0.725464	7
722B-58X-1W	17.9	0.512010	8	-12.25	0.722252	8
731A-42X-1W	18.1	0.512029	5	-11.87	0.723988	7
731B-3X-1W	18.4	0.512035	6	-11.77	0.717237	8
731C-2R-1W	18.9	0.512071	10	-11.06	0.724488	8
731C-2R-2W	19.0	0.512028	5	-11.91	0.724971	8
731C-4R-1W	21.3	0.512005	6	-12.35	0.732802	7
731C-5W-4W	22.0	0.512004	5	-12.36	0.725374	7
731C-6R-1W	24.1	0.512032	7	-11.82	0.729545	7
731C-7W-3W	24.7	0.512081	10	-10.87	0.729158	8
731C-8R-4W	25.3	0.512019	7	-12.08	0.725372	9
731C-9W-6W	25.5	0.512048	7	-11.51	0.721798	7
731C-11W-1W	26.2	0.512016	7	-12.13	0.723202	6
731C-13W-4W	27.0	0.512005	6	-12.35	0.722325	7
731C-14R-2W	27.6	0.512015	6	-12.15	0.723071	9
731C-17R-2W	28.6	0.511993	8	-12.58	0.721050	7
731C-22R-1W	29.3	0.511980	8	-12.84	0.724034	7

* ε_{Nd} values are expressed relative to chondrite values of $^{143}Nd/^{144}Nd=0.512638$: $\varepsilon_{Nd} = (^{143}Nd/^{144}Nd-0.512638) /0.512638 \times 1000$

Table DR5.

Detrital heavy mineral assemblages of samples from ODP Sites 722 and 731

Sample name	Age (Ma)	HMC*	Ap and Ttn	Spinel	Px	Am	Grt	HgM	Ep	ZTR	Total
722B-50X-1W	15.8	5.5	5	4	1	66	10	4	2	8	100
731A-41X-3W	18.0	4.7	3	4	0	43	6	5	25	14	100
731B-4X-1W	18.4	5.4	5	3	2	33	25	4	19	8	100
731C-5W-4W	22.0	4.8	1	0	0	58	22	6	10	3	100
731C-8R-4W	25.3	2.8	10	0	22	7	10	12	23	16	100
731C-11W-1W	26.2	1.1	7	0	13	9	14	9	32	16	100
731C-13W-4W	27.0	1.8	12	0	14	4	10	5	41	14	100
731C-14R-2W	27.6	2.3	8	19	0	0	36	0	12	26	100
731C-17R-2W	28.6	1.0	5	7	0	0	27	5	8	48	100
731C-22R-1W	29.3	1.3	24	4	0	0	15	0	11	45	100

* HMC = Heavy mineral concentration; Ap = apatite; Ttn = titanite; Px = pyroxene; Am = amphibole; Grt = garnet; HgM = high-grade minerals (staurolite, andalusite, kyanite, sillimanite); Ep = epidote; ZTR = ultrastable minerals (zircon, tourmaline, rutile)

Table DR6

Estimations of zircon particles from potential sediment sources to the samples from ODP Sites 722 and 731

Sample name	Age (Ma)	Zircon grains			Zircon budget*		Bulk budget†	
		<200 Ma	>200 Ma	Total	EAP	Himalaya	EAP	Himalaya
722B-50X-1W	15.8	19	94	113	17%	83%	12%	88%
731A-41X-3W	18.0	24	107	131	18%	82%	14%	86%
731B-4X-1W	18.4	17	124	141	12%	88%	9%	91%
731C-5W-4W	22.0	37	112	149	25%	75%	19%	81%
731C-6R-1W	24.1	23	121	144	16%	84%	12%	88%
731C-8R-4W	25.3	34	103	137	25%	75%	19%	81%
731C-11W-1W	26.2	64	81	145	44%	56%	36%	64%
731C-13W-4W	27.0	63	91	154	41%	59%	33%	67%
731C-14R-2W	27.6	24	102	126	19%	81%	14%	86%
731C-17R-2W	28.6	32	93	125	26%	74%	19%	81%
731C-22R-1W	29.3	38	91	129	29%	71%	23%	77%

*Zircon ages <200 Ma are grouped into EAP (Eurasian plate) and >200 Ma are grouped into Himalaya.

†Estimation of bulk budget is based on zircon fertilities of the EAP and Himalaya (Liang et al., 2019, Table DR7)

Table DR7

Estimations of zircon fertilities of EAP and Himalaya based on heavy mineral analysis of detrital samples from local rivers (Liang et al., 2019).

River name	Tectonic units	Sample name	Zircon Fertilities
Hushe	Karakoram	S1749	1.6%
Braldu	Karakoram	S1748	0.9%
Hunza	Karakoram	S1437	0.5%
Hispar	Karakoram	S1438	2.2%
Stagmo	Ladakh	S4426	0.4%
Domkar	Ladakh	S4430	2.4%
Kandia	Kohistan	S1439	0.0%
Swat	Kohistan	S1440	0.2%
	EAP		**1.0%**
Zanskar	Himalaya	S4419	0.9%
Nandihar	Himalaya	S1426	0.6%
	Himalaya		**0.7%**

Table DR8

The lag time and cooling rate calculated from apatite fission track ages of ODP 722 and 731

Sample name	n	Depositional Age (Ma)	±2σ*	Youngest cooling peak age (Ma) †	±2σ	Lag time (m.y.) ‡	Cooling rate (°C/m.y.)§
722B-50X-1W	93	15.8	1.4	19.6	1.5	3.8	28.9
731B-4X-1W	80	18.4	0.2	21.4	1.6	3.0	36.7
731C-5W-4W	70	22.0	1.5	25.9	2.0	3.9	28.2
731C-8R-4W	70	25.3	0.4	28.4	2.2	3.1	35.5
731C-13W-4W	85	27.0	0.4	31.0	2.3	4.0	27.5
731C-22R-1W	74	29.3	0.4	35.0	2.7	5.7	19.3

*The error bars of the depositional ages follow the study on AFT dating of Bengal Fan deposits (Corrigan and Crowley, 1990) who define the uncertainties in the ages of the top and bottom of the 100m-interval which is a normal thickness for turbidite layer.

†Youngest cooling peak ages are from Figure 4A. All samples were counted with a zeta calibration factor $\xi = 343.0 \pm 23$ (Table DR12)

‡Lag time (m.y.) = Youngest cooling peak age (Ma) - Depositional Age (Ma)

§The cooling rate of the potential sources can be calculated by:

$$E = \frac{T_c - T_s}{t_l}$$

Here, E is the cooling rate (°C/m.y.); T_c is the closure temperature of AFT (110 °C); T_s is the surface temperature (0°C); and t_l is the lag time (m.y.).

Table DR9 (Supplemental Excel file).

Compiled zircon U-Pb ages from sediment sources in the Indus River drainage basin.

Table DR10 (Supplemental Excel file).

Compiled Nd-Sr isotopic compositions from sediment sources in the Indus River drainage basin.

Table DR11 (Supplemental Excel file).

Raw data of zircon U-Pb ages of the samples from ODP Sites 722 and 731.

Table DR12 (Supplemental Excel file).

Raw data of apatite fission track ages of the samples from Sites ODP 722 and 731.

Table DR13 (Supplemental Excel file).

Compiled $\delta^{13}C$ and $\delta^{18}O$ records from pedogenic carbonates for deposits in South Asia

References from Data in Figures (1 and 2) and Tables (1~8)

Clift, P.D., Giosan, L., Blusztajn, J., Campbell, I.H., Allen, C., Pringle, M., Tabrez, A.R., Danish, M., Rabbani, M.M., Alizai, A., Carter, A., and Lückge, A., 2008, Holocene erosion of the Lesser Himalaya triggered by intensified summer monsoon: Geology, v. 36, no. 1, p. 79–82, doi: 10.1130/G24315A.1.

Clift, P.D., Zhou, P., Stockli, D.F., and Blusztajn, J., 2019, Regional Pliocene exhumation of the Lesser Himalaya in the Indus drainage: Solid Earth, v. 10, no. 3, p. 647–661, doi: 10.5194/se-10-647-2019.

Corrigan, J.D., and Crowley, K.D., 1990, Fission-Track Analysis of Detrital Apatites from Sites 717 and 718, Leg 116, Central Indian Ocean: Proceedings of the Ocean Drilling Program, Scientific Results, v. 116, p. 75–92.

Li, Y., Clift, P.D., and O'Sullivan, P., 2018, Millennial and centennial variations in zircon U-Pb ages in the quaternary indus submarine canyon: Basin Research, v. 31, no. 1, p. 155–170, doi: 10.1111/bre.12313.

Liang, W., Garzanti, E., Andò, S., Gentile, P., and Resentini, A., 2019, Multimineral Fingerprinting of Transhimalayan and Himalayan Sources of Indus-Derived Thal Desert Sand (Central Pakistan): Minerals, v. 9, no. 8, p. 457.

Prell, W.L., and Niitsuma, N., 1989, Proceedings of the Ocean Drilling Program, Initial Reports, 117: Ocean Drilling Program, College Station, TX.